

Electronic Supporting Information for

**Halide selective anion recognition by an amide-triazolium axle containing
[2]rotaxane**

Nicholas G. White,^a Ana R. Colaço,^b Igor Marques,^b Vítor Félix^b and Paul D. Beer^{a*}

^a *Inorganic Chemistry Laboratory, Department of Chemistry, University of Oxford, South Parks Road, Oxford, United Kingdom, OX1 3QR.*

^b *Departamento de Química, CICECO and Secção Autónoma de Ciências da Saúde, Universidade de Aveiro, 3810-193 Aveiro (Portugal).*

Contents	1
General synthetic remarks	2
NMR and mass spectra of new compounds	3
ROESY NMR spectrum of 7 ·PF ₆	7
Titration protocols	8
Titration binding data	9
Details of X-ray crystallography	10
Details of modelling studies	11
References	17

General synthetic remarks

Unless otherwise stated, chemicals were available commercially, and used as received. Where solvents are specified as “dry,” they were purged with nitrogen and passed through an MBraun MPSP-800 column. NEt_3 was distilled from, and stored over KOH pellets. Water was deionised and microfiltered using a Milli-Q Millipore machine. TBA salts and $[\text{Cu}(\text{CH}_3\text{CN})_4](\text{PF}_6)$ were stored in a vacuum dessicator. TBTA was prepared following the literature procedure^{S1} and stored in a vacuum dessicator. Chromatography was performed on silica gel (particle size: 40–63 μm) or preparative TLC plates (20 × 20 cm, silica thickness: 1 mm).

Routine NMR spectra were recorded on a Varian Mercury 300 spectrometer with ^1H NMR operating at 300 MHz, ^{13}C at 75.5 MHz, ^{19}F at 283 MHz, and ^{31}P at 122 MHz. Some compounds were too poorly-soluble, or not enough compound was synthesised to allow ^{13}C NMR spectra to be recorded on the 300 MHz spectrometer. In these cases, the spectra were collected on a Bruker AVII 500 spectrometer with a 5 mm $^{13}\text{C}(^1\text{H})$ dual cryoprobe with ^{13}C operating at 126 MHz and ^1H operating at 500 MHz. High resolution ESI mass spectra were recorded on a Bruker μTOF spectrometer. High resolution EI mass spectra were recorded on a Waters GCT Classic spectrometer. Low resolution ESI mass spectra were recorded on a Walters LCT premier spectrometer.

NMR spectra of new compounds

Triazole acid 2

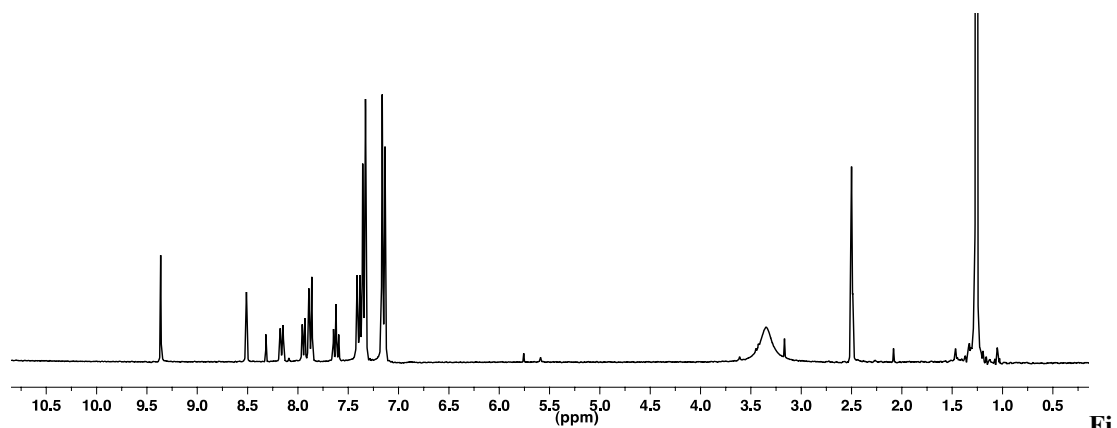


Figure S1. ^1H NMR spectrum of **2** (d_6 -DMSO, 293 K, 300 MHz).

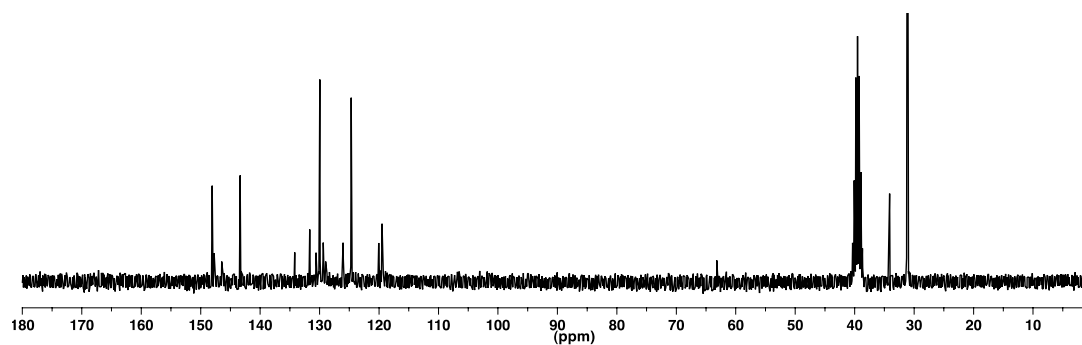


Figure S2. ^{13}C NMR spectrum of **2** (d_6 -DMSO, 293 K, 76 MHz).

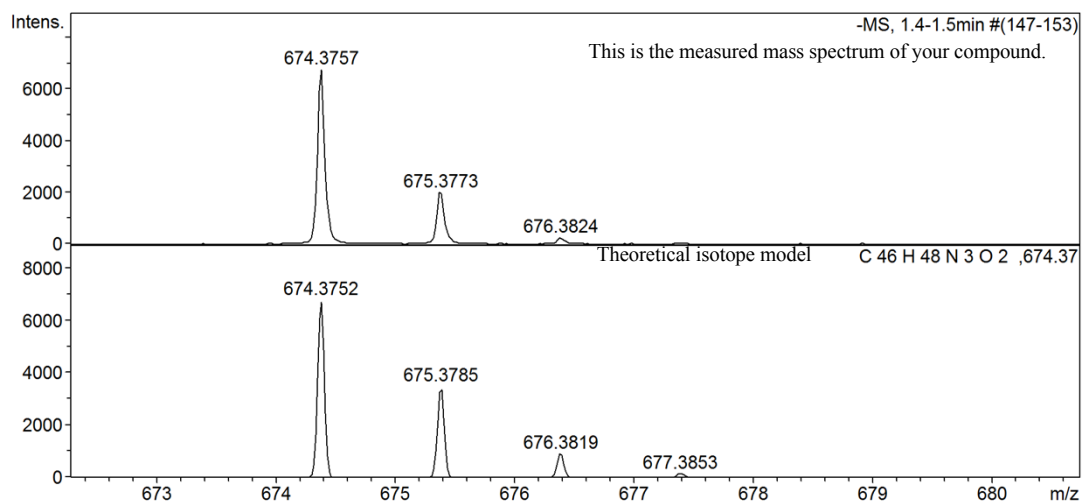


Figure S3. Measured (top) and modelled (bottom) HRESI mass spectrum of **2**.

Triazole axle component 5

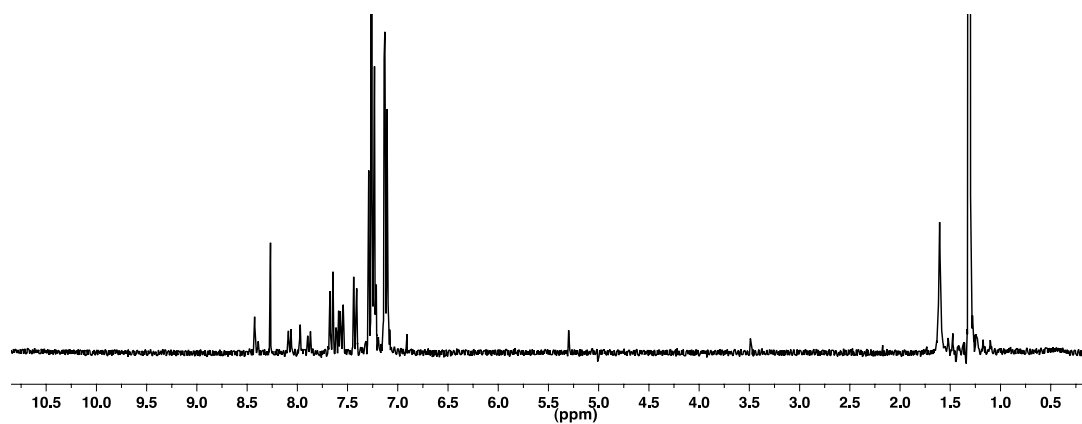


Figure S4. ^1H NMR spectrum of **5** (CDCl_3 , 293 K, 300 MHz).

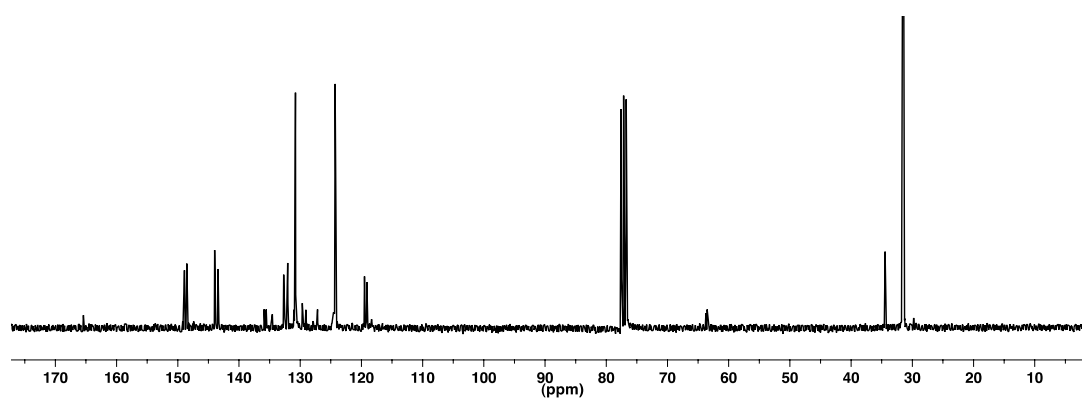


Figure S5. ^{13}C NMR spectrum of **5** (CDCl_3 , 293 K, 76 MHz).

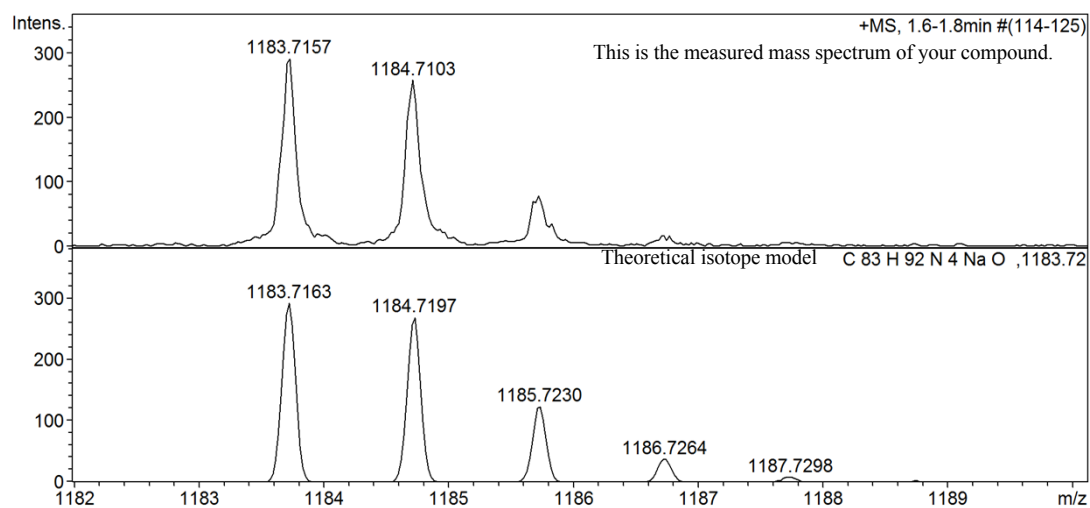


Figure S6. Measured (top) and modelled (bottom) HRESI mass spectrum of **5**.

Triazolium axle component 1·BF₄

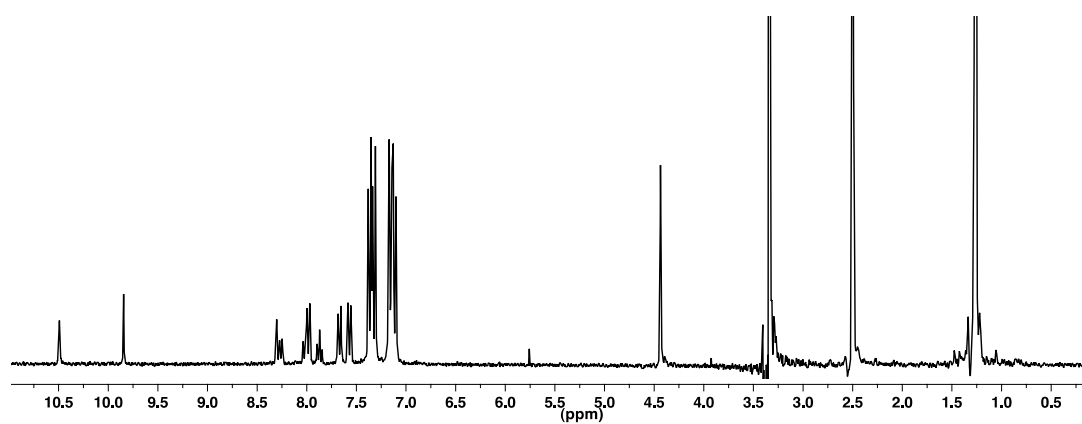


Figure S7. ¹H NMR spectrum of 1·BF₄ (d₆-DMSO, 293 K, 300 MHz).

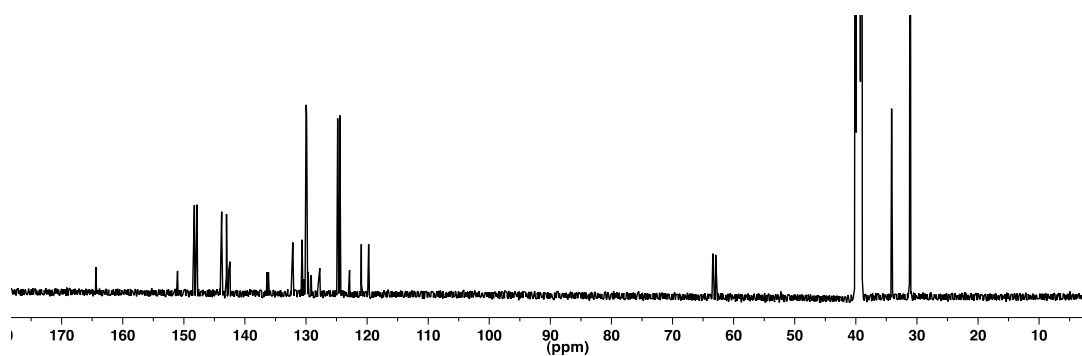


Figure S8. ¹³C NMR spectrum of 1·BF₄ (d₆-DMSO, 293 K, 126 MHz).

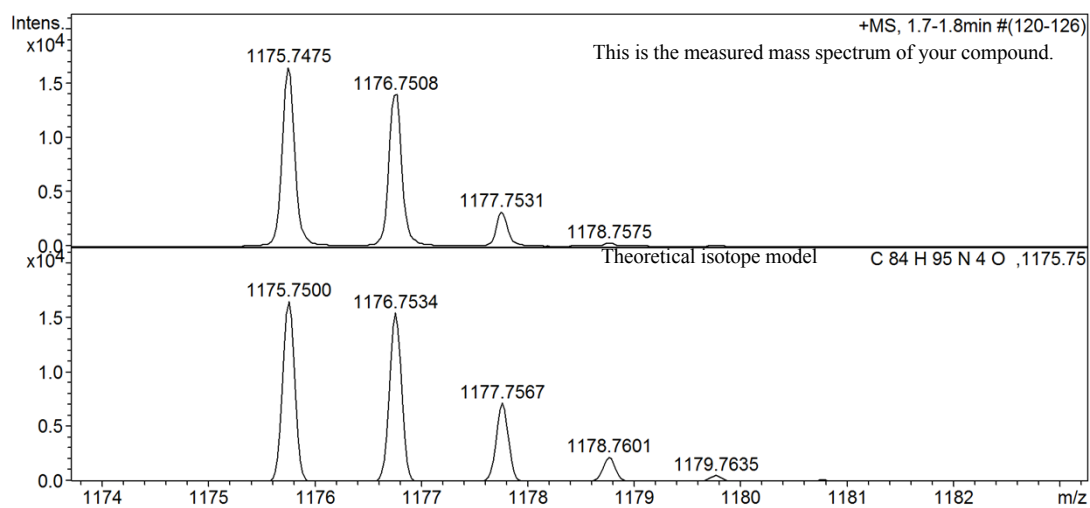


Figure S9. Measured (top) and modelled (bottom) HRESI mass spectrum of 1⁺.

Rotaxane 7·PF₆

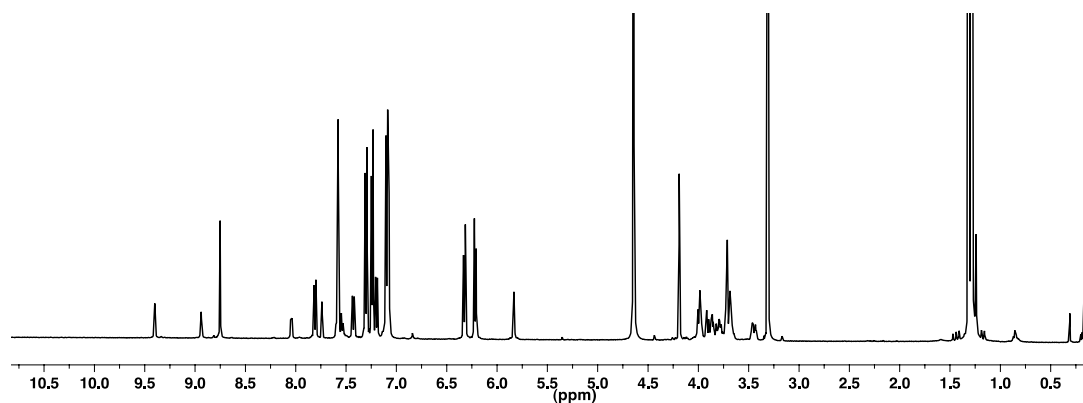


Figure S10. ¹H NMR spectrum of 7·PF₆ (1:1 CDCl₃:CD₃OD, 293 K, 500 MHz).

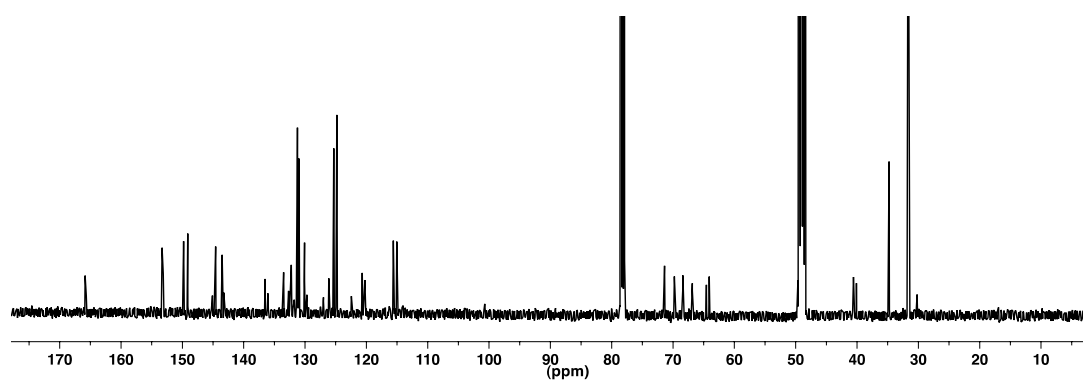


Figure S11. ¹³C NMR spectrum of 7·PF₆ (1:1 CDCl₃:CD₃OD, 293 K, 126 MHz).

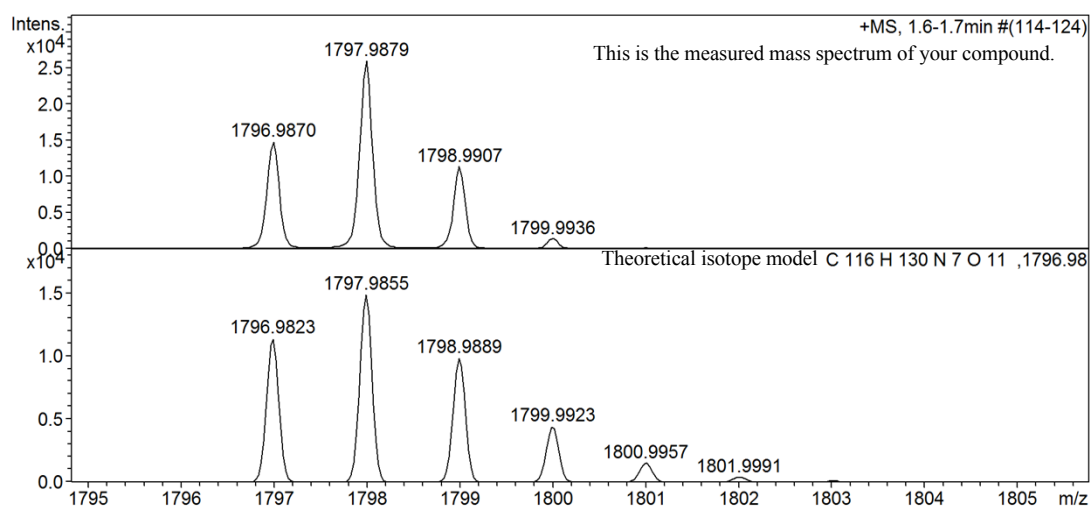


Figure S12. Measured (top) and modelled (bottom) HRESI mass spectrum of 7⁺.

ROESY NMR spectrum of $7 \cdot \text{PF}_6$

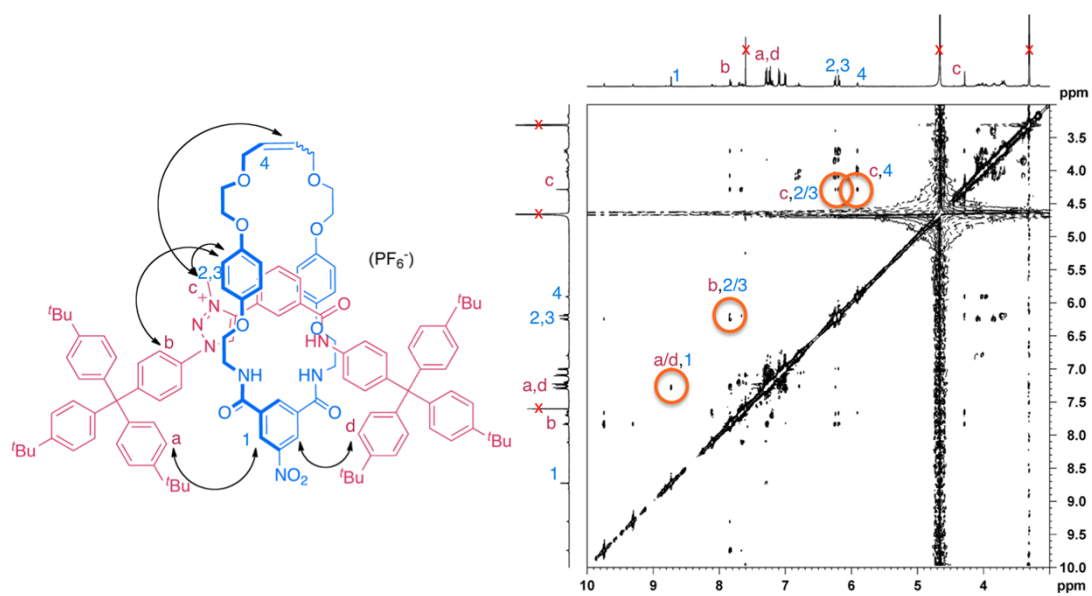


Figure S13. Truncated ROESY NMR spectrum of $7 \cdot \text{PF}_6$ showing selected inter-component couplings; red crosses indicate residual chloroform/methanol/water peaks (1:1 CDCl_3 , 293 K, 500 MHz).

Titration protocols

Spectra for ^1H NMR titrations were recorded at 293 K on a Varian Unity Plus 500 spectrometer with ^1H operating at 500 MHz. Initial sample volumes were 0.50 mL and concentrations were 2.0 mM of host. Solutions (100 mM) of anions as their tetrabutylammonium salts were added in aliquots, the samples thoroughly shaken and spectra recorded. Spectra were recorded at 0, 0.2, 0.4, 0.6, 0.8, 1.0, 1.2, 1.4, 1.6, 1.8, 2.0, 2.5, 3.0, 4.0, 5.0, 7.0 and 10 equivalents. Stability constants were obtained by analysis of the resulting data using the WinEQNMR2^{S2} computer program, monitoring the triazole C–H proton resonance in all cases.

Estimates for the association constant and the limiting chemical shifts were added to the program's input file. The parameters were refined by non-linear least-squares analysis using WINEQNMR2^{S2} to achieve the best fit between observed and calculated chemical shifts. The input parameters for the final chemical shift and association constant were adjusted based on the program output until convergence was reached. Comparison of the calculated and experimental binding isotherms demonstrated that an appropriate model with an appropriate stoichiometry was being used.

Titration binding data

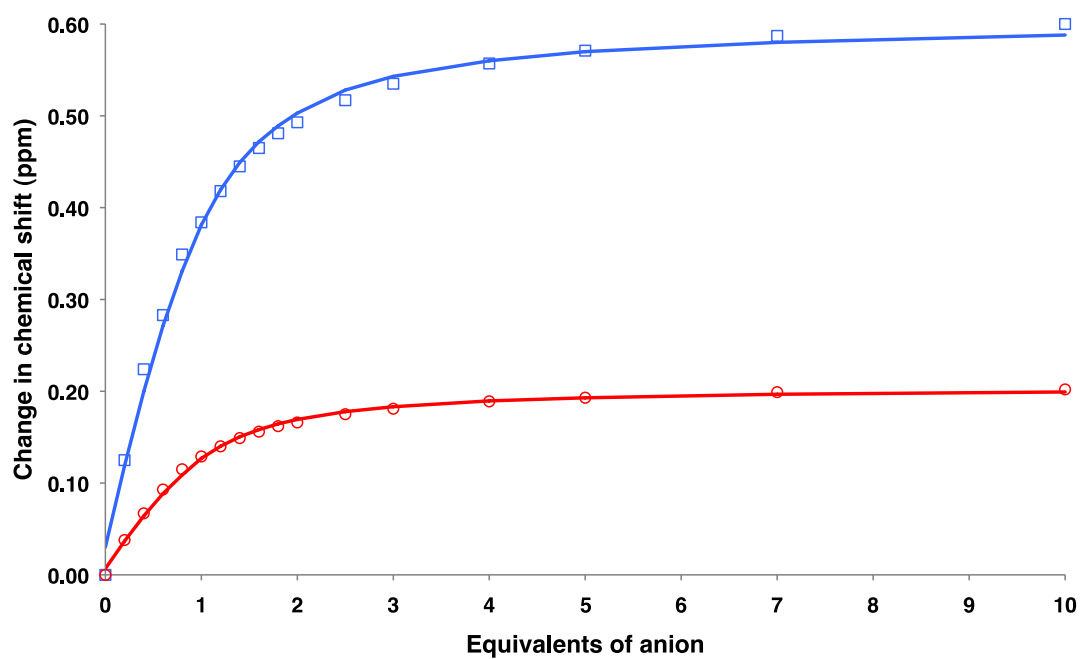


Figure S14. Experimental titration data (points) and fitted binding isotherms (curves) obtained using WINEQNMR2,^{S2} for addition of chloride (top, blue) and bromide (bottom, red) anions to $7\cdot\text{PF}_6$ (1:1 $\text{CDCl}_3:\text{CD}_3\text{OD}$, 293 K, 500 MHz).

X-Ray crystallography details

Crystals were small and extremely weakly diffracting. Synchrotron radiation was used, but even so, numerous reflections were too weak to be observed, particularly at higher angle. The crystals were also found to be twinned – a suitable twin law was found and applied using the ROTAX feature of CRYSTALS.

A large part of the macrocycle ring is disordered – this was modelled over two sites, with the occupancy of each part refined and then fixed (Figure S11). It was necessary to apply restraints to bond distances and angles of the disordered part of the structure to achieve a sensible refinement. Soft restraints were also applied to thermal and vibrational ellipsoid parameters.

Despite the challenges associated with the poor data, the overall structure of the rotaxane can be unequivocally determined.

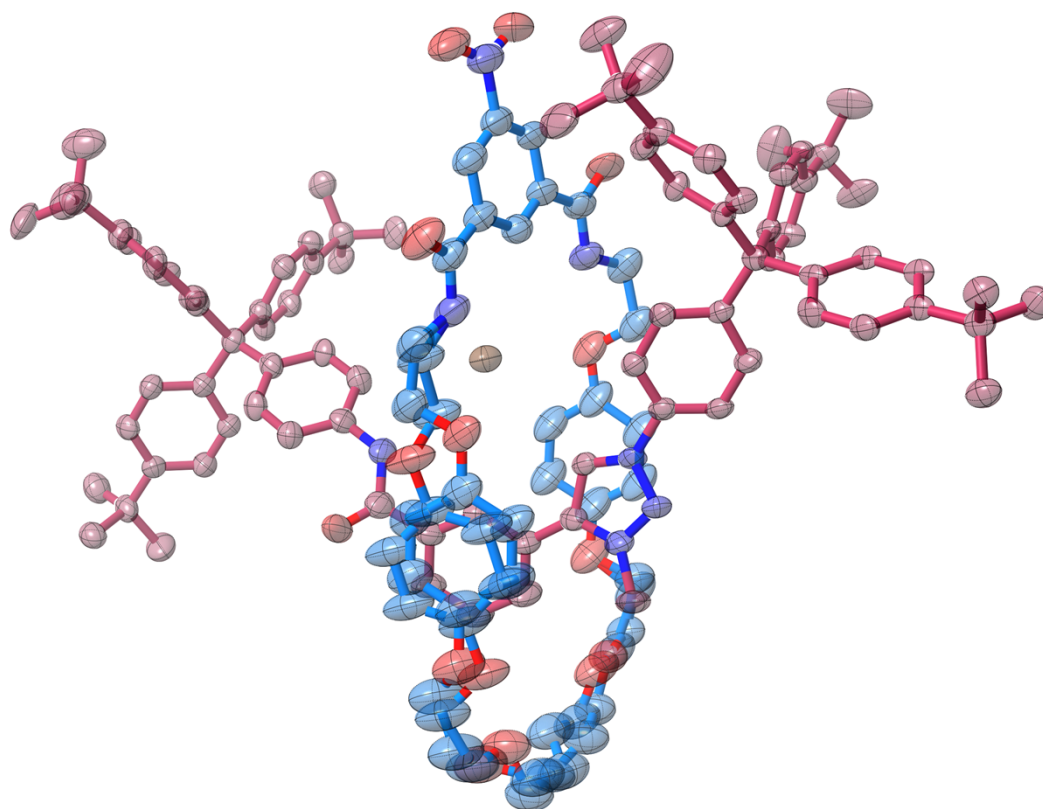


Figure S15. Thermal ellipsoid plot of rotaxane **7·Br** showing macrocycle disorder. Ellipsoids are shown at 50% probability, hydrogen atoms are omitted for clarity.

Molecular modeling details

Computational details

All quantum calculations reported were carried out with Gaussian 09 software package.^{S3}

The electrostatic potential calculations were carried out using the X-ray structures as starting geometries for the axle components and macrocycle. These structures were optimised at B3LYP/6-31G** and, subsequently, single point electrostatic potential energy calculations at the same theory level were performed in order to obtain the electrostatic potential (V_S) mapped onto the electron density surface of the individual molecules. The most positive values ($V_{S,max}$) of V_S were computed using the Wave Function Analysis Program kindly provided by Bulat.^{S4,5} The starting geometries of 3-amido-phenyl-triazolium ($\mathbf{7}_{methyl}^+$), pyridinium bis-triazole ($\mathbf{8}_{methyl}^+$) and pyridinium bis-amide ($\mathbf{9}_{methyl}^+$) axle motifs were obtained by atomic manipulation of the corresponding axle structures, and the $V_{S,max}$ were calculated using the same approach.

Natural Bond Orbital (NBO) analysis was used to assess the strength of the intermolecular hydrogen bonds in model complexes of the axle motifs $\mathbf{7}_{methyl}^+$, $\mathbf{8}_{methyl}^+$ and $\mathbf{9}_{methyl}^+$ with Cl^- , Br^- , OAc^- and $H_2PO_4^-$, which were carried out with NBO program version 3.1^{S6} as implemented in Gaussian 09 software package. This analysis was performed on their previously optimised geometries using the B3LYP functional and the higher basis set 6-311+G**.

Electrostatic energy surfaces of full axle components

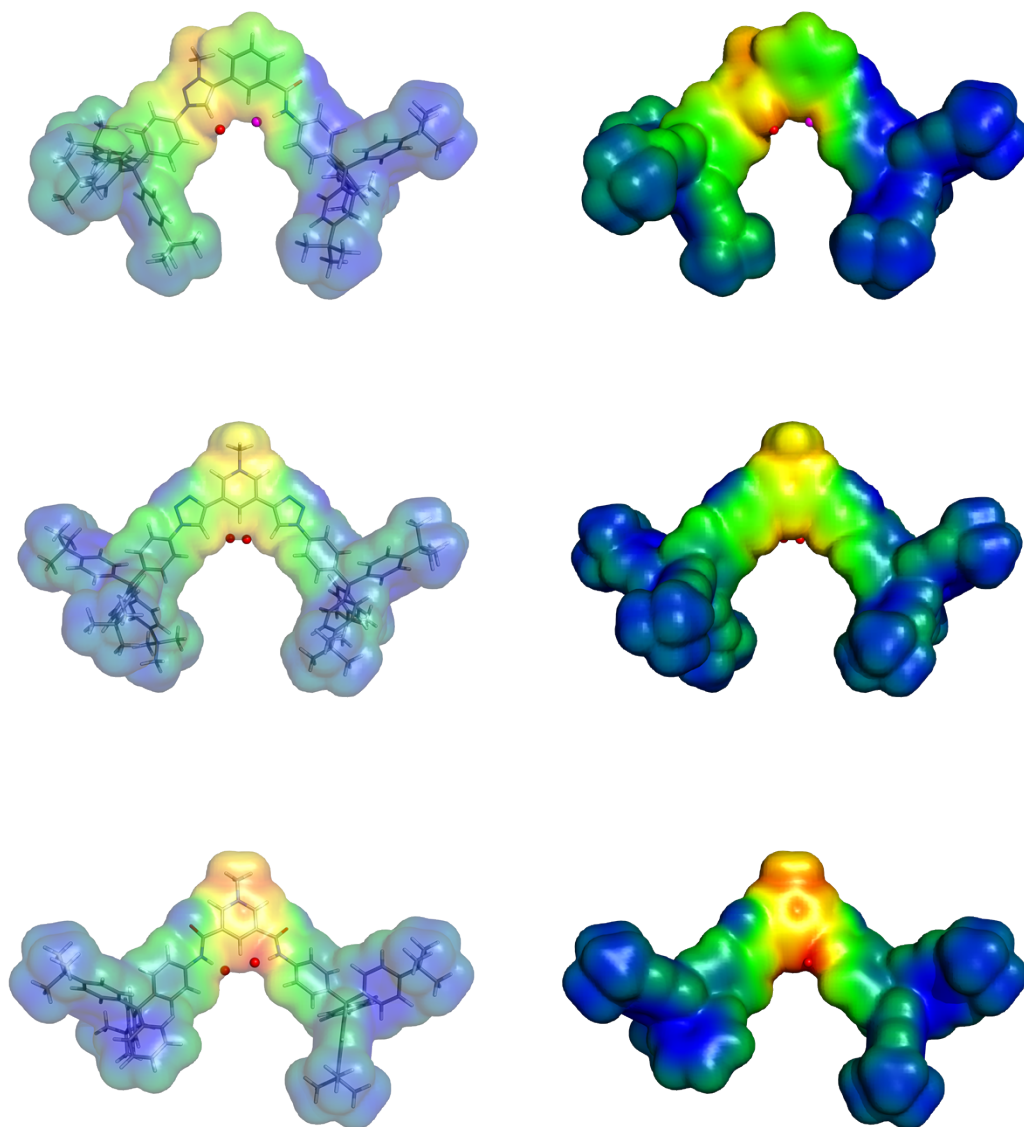


Figure S16. Computed electrostatic potential mapped on the 0.001 electrons/Bohr³ surface of 7⁺ (top), 8⁺ (middle) or 9⁺ (bottom), with colours ranging between blue (< 18.8 kcal mol⁻¹), and red (> 113.0 kcal mol⁻¹). The location of $V_{s,max}$ are illustrated with red and purple dots.

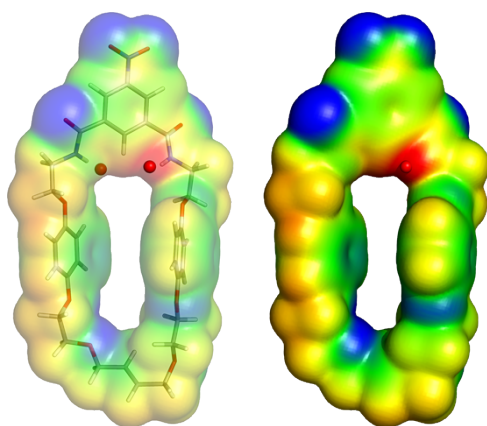


Fig. S17. Computed Electrostatic potential mapped on the 0.001 electrons/Bohr³ surface of the macrocycle, with colours ranging between blue (< -25.1 kcal mol⁻¹), and red (> 31.4 kcal mol⁻¹). The location of $V_{S,max}$ are illustrated with red dots.

DFT optimised geometries of 8^+_{methyl} and 9^+_{methyl} with anions

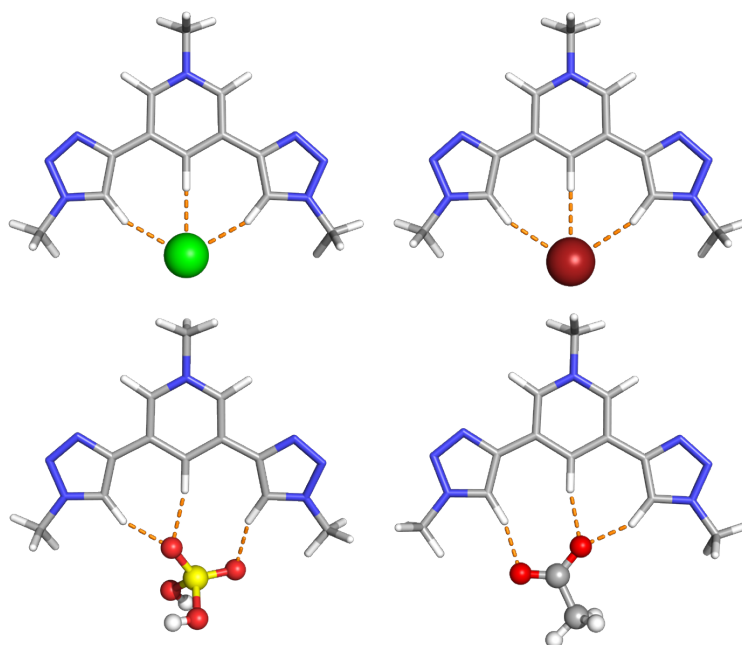


Figure S18. DFT optimised geometries at B3LPY/6-311+G** of the monoatomic (top) and polyatomic (bottom) anions complexes with 8^+_{methyl} axle motif. The hydrogen bonds are drawn as orange dashed lines.

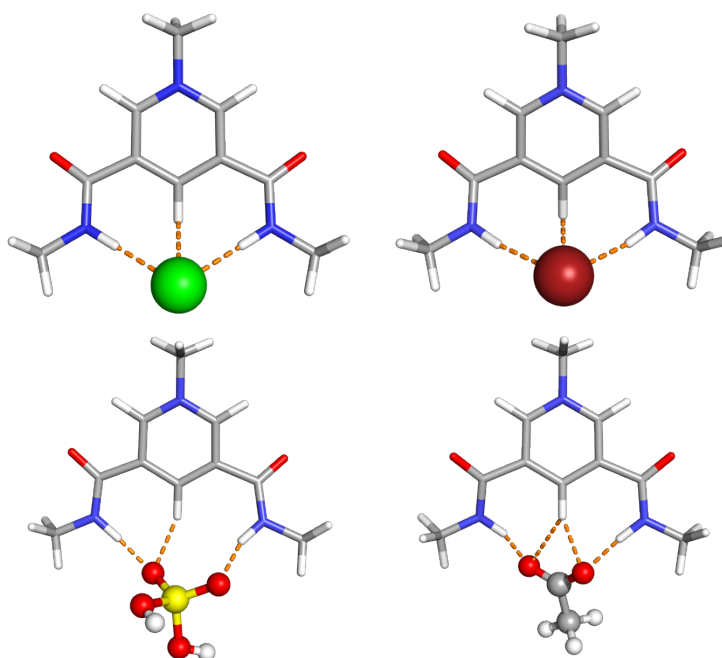


Figure S19. DFT optimised geometries at B3LPY/6-311+G** of the monoatomic (top) and polyatomic (bottom) anions complexes with 9^+_{methyl} axle motif. The hydrogen bonds are drawn as orange dashed lines.

The $\mathbf{9}_{\text{methyl}}^+$ model ligand establishes with the chloride anion two short and almost linear N–H \cdots Cl $^-$ hydrogen bonds (N \cdots Cl $^-$ distances of 3.219 and 3.220 Å) assisted by a third one formed with the *ortho* hydrogen from central pyridinium central unit (C \cdots Cl $^-$ distance of 3.144 Å). The same number of hydrogen bonds was observed in the chloride complexes with $\mathbf{7}_{\text{methyl}}^+$ and $\mathbf{8}_{\text{methyl}}^+$. The former complex displays C_{triazolium}–H \cdots Cl $^-$ and N–H \cdots Cl $^-$ asymmetric bonding interactions with N \cdots Cl $^-$ and C \cdots Cl $^-$ distances of 3.337 and 3.191 Å, respectively. By contrast, the complex with $\mathbf{8}_{\text{methyl}}^+$ exhibits two nearly symmetric C_{triazole}–H \cdots Cl $^-$ hydrogen bonds with longer C \cdots Cl $^-$ distances of 3.418 and 3.417 Å. These hydrogen bonds dimensions lead to E^2 energies for the three chloride anion associations following the order $\mathbf{9}_{\text{methyl}}^+ > \mathbf{7}_{\text{methyl}}^+ > \mathbf{8}_{\text{methyl}}^+$, which is consistent with the computed $V_{\text{S,max}}$ for these three moieties and with experimental binding selectively reported in Table 2 for the corresponding interlocked hosts. Equivalent structural and energetic trends are observed for bromide complexes with these fragments. In other words, the hydrogen bonds distances follow the order $\mathbf{9}_{\text{methyl}}^+ < \mathbf{7}_{\text{methyl}}^+ < \mathbf{8}_{\text{methyl}}^+$, while for corresponding E^2 values the order is reversed. Therefore, it is expected that the interlocked host $\mathbf{9}^+$ has a higher affinity also for the bromide anion in spite of the absence of experimental binding data.

The same rationale cannot be straightforwardly applied to the oxoanion complexes because they present multiple hydrogen bonds, ranging between three and four (Figures 5, S13 and S14). Overall, for a given central axle motif, the dimensions of the hydrogen bonds established with either H₂PO₄ $^-$ or OAc $^-$ are comparable (see Tables S1-S3). However, the synergetic effect of these binding interactions yields large E^2 values for complexes of $\mathbf{8}_{\text{methyl}}^+$, and $\mathbf{9}_{\text{methyl}}^+$ with dihydrogen phosphate and acetate, which comes in agreement with the experimentally observed affinity of the interlocked hosts $\mathbf{8}^+$ and $\mathbf{9}^+$, as particularly evident from the binding constant of $\mathbf{9}\cdot\text{H}_2\text{PO}_4$. In contrast, the lower E^2 values computed for oxoanion $\mathbf{7}_{\text{methyl}}^+$ complexes corroborate the negligible experimental anion recognition observed between interlocked host $\mathbf{7}^+$ and dihydrogen phosphate and acetate anions.

Table S1. Hydrogen bond dimensions with C/N \cdots X distances in Å and C/N-H \cdots X angles in degrees (italicised) for the associations between **7_{methyl}⁺** and Cl⁻, Br⁻, H₂PO₄⁻ and OAc⁻.^a

Anion	Axle binding units		
	N _{amide} -H	C _{isophthalamide} -H	C _{triazolium} -H
Cl ⁻	3.377, 169.8	3.528, 156.0	3.191, 159.7
Br ⁻	3.575, 168.0	3.726, 159.2	3.328, 150.6
H ₂ PO ₄ ⁻	2.896, 176.5	3.041, 153.9	3.186, 142.7; 3.175, 128.1
OAc ⁻	2.879, 175.6	3.092, 159.0	2.914, 144.3; 3.294, 139.7

^a X is a halide anion or an oxygen atom either from OAc⁻ or H₂PO₄⁻.

Table S2. Hydrogen bond dimensions with C \cdots X distances in Å and C-H \cdots X angles in degrees (italicised) for the associations between **8_{methyl}⁺** and Cl⁻, Br⁻, H₂PO₄⁻ and OAc⁻.^a

Anion	Axle binding units		
	C _{triazole} -H	C _{isophthalamide} -H	C _{triazole} -H
Cl ⁻	3.418, 157.1	3.386, 179.7	3.417, 157.1
Br ⁻	3.573, 159.5	3.589, 179.5	3.573, 159.5
H ₂ PO ₄ ⁻	2.936, 153.9	3.116, 166.9	2.976, 160.8
OAc ⁻	2.924, 152.3	3.064, 168.0	2.948, 166.1

^a X is a halide anion or an oxygen atom either from OAc⁻ or H₂PO₄⁻.

Table S3. Hydrogen bond dimensions with N \cdots X distances in Å and N-H \cdots X angles in degrees (italicised) for the associations between **9_{methyl}⁺** and Cl⁻, Br⁻, H₂PO₄⁻ and OAc⁻.^a

Anion	Axle binding units		
	N _{amide} -H	C _{isophthalamide} -H	N _{amide} -H
Cl ⁻	3.219, 179.8	3.144, 125.9	3.220, 179.8
Br ⁻	3.381, 170.7	3.119, 101.3	3.382, 170.7
H ₂ PO ₄ ⁻	2.691, 175.9	3.065, 154.5	2.711, 161.9
OAc ⁻	2.686, 163.2	3.088, 160.3; 3.474, 135.9	2.709, 173.9

^a X is a halide anion or an oxygen atom either from OAc⁻ or H₂PO₄⁻.

References

- ^{S1} B.-Y. Lee, S. R. Park, H. B. Jeon, K.S. Kim, *Tetrahedron Lett.*, 2006, **47**, 5105.
- ^{S2} M. J. Hynes, *J. Chem. Soc., Dalton Trans.*, 1993, 311.
- ^{S3} M. J. Frisch, G. W. Trucks, H. B. Schlegel, G. E. Scuseria, M. A. Robb, J. R. Cheeseman, G. Scalmani, V. Barone, B. Mennucci, G. A. Petersson, H. Nakatsuji, M. Caricato, X. Li, H. P. Hratchian, A. F. Izmaylov, J. Bloino, G. Zheng, J. L. Sonnenberg, M. Hada, M. Ehara, K. Toyota, R. Fukuda, J. Hasegawa, M. Ishida, T. Nakajima, Y. Honda, O. Kitao, H. Nakai, T. Vreven, J. A. Montgomery Jr, J. E. Peralta, F. Ogliaro, M. Bearpark, J. J. Heyd, E. Brothers, K. N. Kudin, V. N. Staroverov, R. Kobayashi, J. Normand, K. Raghavachari, A. Rendell, J. C. Burant, S. S. Iyengar, J. Tomasi, M. Cossi, N. Rega, J. M. Millam, M. Klene, J. E. Knox, J. B. Cross, V. Bakken, C. Adamo, J. Jaramillo, R. Gomperts, R. E. Stratmann, O. Yazyev, A. J. Austin, R. Cammi, C. Pomelli, J. W. Ochterski, R. L. Martin, K. Morokuma, V. G. Zakrzewski, G. A. Voth, P. Salvador, J. J. Dannenberg, S. Dapprich, A. D. Daniels, O. Farkas, J. B. Foresman, J. V. Ortiz, J. Cioslowski and D. J. Fox, *Gaussian 09*, Revision A.01, Gaussian, Inc., Wallingford CT, 2009.
- ^{S4} F. A. Bulat and A. Toro-Labbé, *WFA: A suite of programs to analyse wavefunctions*, unpublished work.
- ^{S5} F. A. Bulat, A. Toro-Labbe, T. Brinck, J. S. Murray and P. Politzer, *J. Mol. Model.*, 2010, **16**, 1679.
- ^{S6} *NBO Version 3.1*, E. D. Glendening, A. E. Reed, J. E. Carpenter and F. Weinhold.